

## Numerical Investigations of Coupling a Vacuum Membrane Desalination System with a Salt Gradient Solar Pond

Samira Ben Abdallah\*, Nader Frikha and Slimane Gabsi

Samira Ben Abdallah, Research Unit of Environment, Catalysis and Analysis Processes, University of Gabes, National Engineering school of Gabès, Street Omar Ibn ElKhattab, 6029 Gabès, Tunisia

### Abstract

This work proposes new configurations for the desalination of salt water using systems based on coupling of membrane distillation with solar energy. This study is a comparison between two coupling configurations of the vacuum membrane distillation (VMD) hollow fiber module with salinity gradient solar pond (SGSP). The first configuration is a module membrane in series with SGSP and the second one is a hollow fiber module immersed in the SGSP. Two models describing the heat and mass transfer in the hollow fiber module and in the SGSP will be developed. The coupling of the two models allows the determination of the instantaneous variation of temperature and salinity in the SGSP and the permeate flow variation. A comparison of each module production was carried out. The mathematical model shows that the immersed module production presents more than one and a half times that of the separated module, their production reached  $75 \text{ kg}\cdot\text{day}^{-1}$  per  $\text{m}^2$  of the membrane in the third year. Thus, immersing the module in the solar pond improves the performance of the hollow fiber module.

**Keywords:** Desalination; Hollow fiber module; Modeling; Solar pond

### Abbreviations

### Nomenclature

AM: Sun's path; alt: altitude;  $C_c$ : Conversion factor of the isotropic fraction;  $C_p$ : The specific heat capacity of the water;  $D_i$ : Diffuse radiation on a flat surface;  $D$ : Coefficient of salt diffusion;  $D_h$ : Horizontal diffuse radiation;  $F$ : Fraction of isotropic diffusion;  $G_h$ : Horizontal global radiation;  $h$ : Height of the sun;  $I_0$ : Incidence solar radiation;  $P_s$ : Vapor pressure;  $P_{\text{vacuum}}$ : Vacuum pressure;  $S$ : Salinity;  $Q_m$ : Mass flow;  $Q$ : Heat flow;  $R$ : The ideal gas constant;  $T$ : Temperature;  $X_{\text{NaCl}}$ : Salt molar fraction;  $I_n$ : Normal incidence solar radiation

### Greek letters

$\alpha_d$ : Distance correction coefficient;  $\alpha_{th}$ : Heat expansion coefficient;  $\alpha_{\text{eau/NaCl}}$ : Water activity coefficient;  $\beta$ : Disturbing factor;  $\beta_m$ : Expansion coefficient;  $\epsilon$ : Membrane porosity;  $\Phi$ : Inclination angle;  $\lambda$ : Heat conductivity;  $\mu$ : Dynamic viscosity;  $\mu_{ex}$ : Extension coefficient;  $\theta_{inci}$ : Angle of incidence;  $\rho$ : The salt water density;  $\tau$ : Membrane tortuosity

### Indices

acc: accumulated; amb: ambient; abs: absorbed; f: feed; o: out; sw: Sea water

### Introduction

The VMD process is based on the evaporation of solvents through hydrophobic porous membranes promoted by applying vacuum or low pressure on the permeate side [1]. Vacuum is applied in the permeate side of the membrane module by means of a vacuum pump. The applied vacuum pressure is lower than the saturation pressure of volatile molecules to be separated from the feed solution. Permeate condensation takes place outside the module, inside a condenser [2]. This configuration presents a high permeate flow compared to other membrane distillation (MD) configurations, in addition to advantages of low thermal conduction loss [3-5].

MD was considered as a promising technology and has appeared as a process more attractive than any other popular separation process

due to its lower operating temperatures and hydrostatic pressures [6]. Additionally, MD is capable of integrating with various renewable energy sources such as solar energy, geothermal energy and waste heat source [7,8]. The utilization of the renewable energy is worth further research in order to bring the technology closer to the process intensification. So far, the solar energy has been frequently studied in MD by many researchers [9-12]. However, MD requires high heat energy [13]. Being capable of directly using solar thermal energy, the solar membrane distillation desalination system has developed as a promising green technology to reduce the water resource problem [14]. Saffarini et al. have shown that heater systems costs account for over 70% of the total cost for all systems, suggesting the desirability of using alternative sources of thermal energy, such as solar energy [15].

Based on different methods used to impose a vapor pressure difference on either membrane side to drive the permeate flow, there are essentially four types of membrane distillation configurations: direct contact membrane distillation (DCMD), sweeping gas membrane distillation (SGMD), air gap membrane distillation (AGMD) and vacuum membrane distillation (VMD). The majority of research studies concern the coupling of solar collectors with the other configurations of the MD such as DCMD [14,16,17] and AGMD [18,19]. In desalination, the AGMD, the DCMD and the VMD configurations have been successfully applied, providing fresh water as permeate [12,18,20]. Wang et al. were among the first researchers to couple VMD with solar energy [18]. Their study shed the light on a designed and tested solar-heated hollow-fiber-based VMD system. The largest permeate flux obtained is  $32.19 \text{ L}\cdot\text{h}^{-1}$  per  $\text{m}^2$  of membrane with an  $8 \text{ m}^2$  solar energy

**\*Corresponding author:** Samira Ben Abdallah, Research Unit of Environment, Catalysis and Analysis Processes, University of Gabes, National Engineering school of Gabès, Street Omar Ibn ElKhattab, 6029 Gabès, Tunisia, Tel: 216-75-396-955; E-mail: [abdallahsamira@yahoo.com](mailto:abdallahsamira@yahoo.com)

Received June 02, 2016; Accepted July 29, 2016; Published August 02, 2016

**Citation:** Abdallah SB, Frikha N, Gabsi S (2016) Numerical Investigations of Coupling a Vacuum Membrane Desalination System with a Salt Gradient Solar Pond. J Fundam Renewable Energy Appl 6: 213. doi:10.4172/20904541.1000213

**Copyright:** © 2016 Abdallah SB, et al. This is an open-access article distributed under the terms of the Creative Commons Attribution License, which permits unrestricted use, distribution, and reproduction in any medium, provided the original author and source are credited.

collector. The existing configurations are essentially coupled with flat plate collectors and the module was separated to the solar collector. But for the other DM configurations the only coupling with a solar pond is carried out by Nakao et al. [12], which study the utilization of DCMD coupled to a salt gradient solar pond. So the coupling of a flat membrane module separated from the pond was realized. This study shows that the module production reached 2 l/m<sup>2</sup>/hr at the end of June, 2014. Therefore, Mericq et al. [21] studied the possibility of submerging the plate DMV membrane in the SGSP. The use of SGSP does not only seem to be the most interesting solution but also allows a high permeate flux to be reached with membrane fed by waters from lower convective zone (LCZ) of the SGSP. The study of different coupling configurations has confirmed the benefits of the membrane module immersion in the solar collector [18,22-24]. This possibility reduces heat loss and has a compact installation, which leads to improved productivity.

This research work accounts for the possibility of coupling the VMD membrane module with an SGSP. It presents a follow-up of the hollow fiber module production along three years. It also provides a comparison of the water production of two coupling possibilities, the first of which is a module fed with SGSP (Figure 1A) and the second one is a hollow fiber module immersed in the SGSP (Figure 1B). The latter is developed in order to minimize the heat loss and maximize water production. The approach presented in this paper was used to choose the most efficient coupling possibility.

### Modeling

The desalination system is composed of an SGSP and a hollow fiber module. Vacuum membrane distillation is a complicated physical process in which both heat and mass transfers are involved. Indeed, the coupling of the heat and mass transfer equations in the module and the SGSP leads to the establishment of a model describing the functioning of each configuration. The model was developed to calculate the effect of the solar energy on the permeate flux. The variations of the temperature and product distillate during the day were determined.

### Hollow fiber module

The membrane module is a hollow fiber membrane which can have a large effective area compared with other membrane module types. The hollow fiber module configuration is external-internal. The feed solution flows from outside the hollow fibers and the permeate is collected inside the hollow.

MD is a thermally driven process based on the principle of vapor/liquid equilibrium and coupled heat and mass transfer [18]. The heat transfer simultaneously occurs with mass transfer whose process influences the rate and coefficients of the heat transfer process, giving birth to a complex heat transfer model [23]. The transfer through the membrane is caused by a partial pressure difference on either side of the membrane. The vapor water molecule was transported through

the membrane pores from the higher pressure to lower pressure side. Generally in the VMD the vapor water molecules transfer through the membrane pores is given by the mechanism of Knudsen diffusion where the mean free path of the molecules is very large relative to the average pore [9,25-27]. Indeed in VMD, the mean free path of water can reach relatively high values. Then molecule-pore wall collisions are dominant in membranes with small pores. In addition Knudsen diffusion dominates in VMD if the vacuum is sufficiently pushed. In our case we used small pore size membrane (less than 0.45 microns) and a very high vacuum does not exceed the 4000 Pa. So the diffusion of the vapor through the membrane pores according to a Knudsen mechanism.

The water vapor flux through the internal interface membrane-water (kg.s<sup>-1</sup>.m<sup>-2</sup>) is described by the following equation:

$$J_v = K_m \Delta P \quad (1)$$

The driving force of the pressure difference  $\Delta P$  can be expressed as follows:

$$\Delta P = P_i - P_{vacuum} \quad (2)$$

Partial pressure  $P_i$  was written as a function of the activity coefficient and the interfacial concentration.

$$P_i = \alpha_{water/NaCl} (1 - X_{NaCl}) P_s \quad (3)$$

$\alpha_{water/NaCl}$  is the water activity coefficient. This coefficient depends on the water concentration in the treated solution [25].

$$\alpha_{water/NaCl} = 1 - 0.5 X_{NaCl} - 10 X_{NaCl}^2 \quad (4)$$

and  $P_s$  is the interfacial vapor pressure of pure water and can be evaluated using the Antoine equation:

$$= \exp\left(23.238 - \frac{3841}{T_i - 45}\right) \quad (5)$$

where  $T_i$  is the corresponding interfacial temperature in Kelvin.

The coefficient of the membrane permeability or the Knudsen permeability  $K_m$  can be related to the membrane structural properties such and the membrane interface temperature ( $T_i$ ) [9,25,26].

$$K_m = \frac{2 \varepsilon r_p}{3 \tau e_m} \frac{1}{R T_i} \sqrt{\frac{8 R T_i}{\pi}} \quad (6)$$

So

$$J_v = K_m \left[ \alpha_{eau/NaCl} (1 - X_{NaCl}) \exp\left(23.238 - \frac{3841}{T_i - 45}\right) - P_{vacuum} \right] \quad (7)$$

The mass transfer inside the module is coupled with a heat transfer through the membrane. The establishment of a rigorous model describing the heat and mass transfer inside the hollow fibre module is very complex. Based on some assumptions and the heat transfer equation for a flowing liquid in a cylindrical conduct, a model

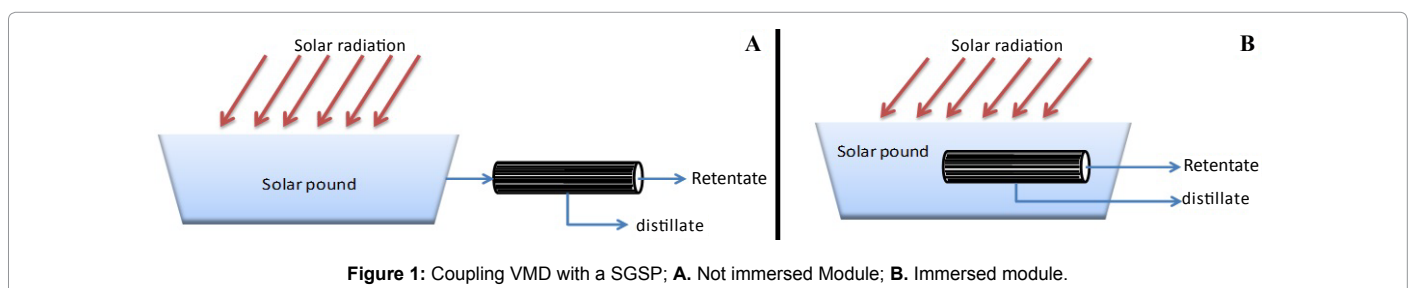


Figure 1: Coupling VMD with a SGSP; A. Not immersed Module; B. Immersed module.

describing the heat and mass transfer in the hollow fiber module was developed [22,24].

To solve the set of model equations we have used of a program using the Matlab calculation software which allows the equations to be presented in the obtained model. The resolution is fully developed by the Ruge Kutta method using the predefined function in Matlab ode 23. This function is executed to solve non-stiff differential equations, low order method.

The obtained model allows to determine the temperature profile inside the module, the module output temperature as well as the flow of distillate produced as a function of different parameters.

### Solar radiation model

The study of solar radiation is the starting point of any solar energy investment. A model describing the different irradiations depending on climatic parameters was developed. This calculus is based on the EUFRAT model which, in turn, is based on the synthesis of various research works, especially those Brichambant, Kasten and Hay [28]. The atmosphere does not transmit the entire solar radiation to the ground:

- Direct radiation is the one that passes through the atmosphere without modification. This radiation at normal incidence is determined from the following equation:

$$I_n = I_0 \alpha_d \exp\left[\frac{-AM \beta}{0.9 AM + 9.4}\right] \quad (8)$$

with AM the sun's path that is given by the following expression:

$$AM = \frac{(1-0.1 \text{ alt})}{\sinh} \quad (9)$$

- The global radiation on a horizontal plane which is the sum of direct and diffuse radiation is described by the following equation:

$$G_h = \alpha_d (1270-56 \beta) \sin(h) \frac{\beta+36}{33} \quad (10)$$

- The diffuse radiation is the part of the solar radiation diffused by the solid or liquid particles suspended in the atmosphere. It has no preferred direction.

The diffuse radiation is determined from the global radiation:

$$D_h = G_h - I_n \sin(h) \quad (11)$$

The diffuse radiation on a flat surface inclined at an angle ( $\Phi$ ) relative to the horizontal (the tilt angle) and oriented to a direction at an angle  $\theta_{inci}$  with the South (incidence angle) is determined using a conversion factor of the isotropic fraction:

$$C_c = \frac{1 + \cos \phi}{2} \quad (12)$$

So

$$\text{If } \frac{\theta_{inci}}{\sin h} > C_c \text{ we have } D_i = D_h \left[ F C_c + \frac{(1-F) \theta_{inci}}{\sinh} \right] \quad (13)$$

$$\text{If } \frac{\theta_{inci}}{\sin h} \leq C_c \text{ we have } D_i = D_h C_c \quad (14)$$

with F as the fraction of isotropic diffusion:  $F = 1 - \frac{I_n}{I_0 \alpha_d}$  (15)

Then, the global radiation on an inclined plane is deduced as the sum of two terms:

$$G_i = I_n \cos \theta_{inci} + 0.2 D_i G_h \frac{(1 - \cos \phi)}{2} \quad (16)$$

The resolution of these equations was carried out using a program that is developed on the Matlab calculation software. The simulation of this program allows us to determine the different types of radiation (direct, diffuse and global) for a given day.

### SGSP model

Practically the solar pond consists of three distinct zones as shown in Figure 2. The first zone, located at the top of the pond, contains the low density saltwater mixture. This zone is called the upper convective zone (UCZ) which is the absorption and transmission region. The second zone which contains a variation of salinity increasing with depth is the gradient zone or non-convective zone (NCZ). This zone acts as an insulator to prevent heat from escaping to the UCZ, maintaining higher temperatures at lower zones. The bottom zone is the heat storage zone or lower convective zone (LCZ) with uniform salinity.

Solar ponds produce relatively low grade thermal energy (less than 100°C) and are generally considered suitable for thermal distillation processes. The solar pond is subjected to solar radiation and heat exchange only through its upper surface. It is assumed that the pond is a priori 'artificially stabilized' so that the convection currents can be considered non-existing and remains as such during the entire period of time under consideration [29].

The energy balance on the volume element of the pond ( $\Delta V = A_{pond} \Delta x$ ) is given by the following equation:

$$Q_{acc}(t, x) = Q_f(t, x) - Q_o(t, x) + Q_{abs}(t, x) \quad (17)$$

This equation reflects that the heat flow accumulated in the volume element is equal to the sum of the inlet flow and absorbed flow minus the out flow.

The energy flow accumulated in the pond volume element (saltwater) is given by the equation:

$$Q_{acc}(t, x) = \Delta x \frac{\partial(\rho_{sw} C_p T_{sw}(t, x))}{\partial t} \quad (18)$$

The difference between the feed and output energy flow is expressed by the following equation:

$$Q_f(t, x) - Q_o(t, x) = \lambda_{sw} A_{pond} \frac{\partial^2 T_{sw}(t, x)}{\Delta^2 x} \Delta x \quad (19)$$

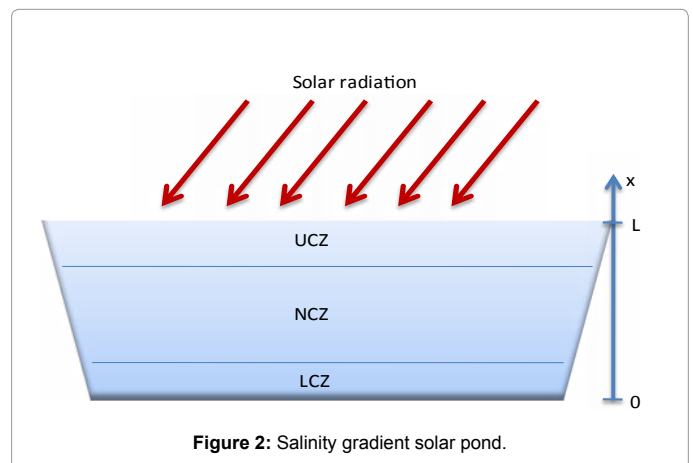


Figure 2: Salinity gradient solar pond.

The absorbed energy flow is the rate of energy production in a salt water layer, which results from the solar radiation absorption.

$$Q_{abs}(t, x) = \frac{dI}{dx} A_{pond} \Delta x \quad (20)$$

I is the solar flux received by the higher interface of the pond. The term  $\frac{dI}{dx}$  represents, in fact, the rate of energy generation per unit volume in a water layer, which results from the solar radiation absorption. In the present study, we have assumed that the amount of solar radiation, mostly in short wave radiation ranges, reaching the depth x within the pond, suffers an exponential decay as follows [30]:

$$I = 0,6 G_i e^{-\mu_{ex}(L-x)} \quad (21)$$

Where  $G_i$  is the solar radiation incident on the water free surface, which is assumed to be normal to that surface,  $\mu_{ex}$ , called the extinction coefficient, represents the transparency of the saline solution and L the solar pond depth.

The absorbed flow expression is then as follows [31]:

$$Q_{abs}(t, x) = 0,6 \mu_{ex} G_i e^{-\mu_{ex}(L-x)} A_{pond} \Delta x \quad (22)$$

The heat transfer process within the solar pond is governed by the following general equation:

$$\frac{\partial(\rho_{sw} C p_{sw} T_{sw}(t, x))}{\partial t} = \lambda_{sw} \frac{\partial^2 T_{sw}(t, x)}{\partial^2 x} + 0,6 \mu_{ex} G_i e^{-\mu_{ex}(L-x)} \quad (23)$$

In addition, the mass balance in the volume element of the pond is expressed by the following equation:

$$Q_{m,acc}(t, x) = Q_{m,x+dx}(t, x) - Q_{m,x}(t, x) \quad (24)$$

The mass flow in the pond is described by Fick's law:

$$Q_{m,x} = -D A_{pond} \frac{\partial(\rho_{sw} S)}{\partial x} \quad (25)$$

Then, the difference between the inlet and exit mass flow is expressed by the following equation:

$$Q_{m,acc} = D A_{pond} \frac{\partial^2(\rho_{sw} S)}{\partial^2 x} \Delta x \quad (26)$$

The accumulated salt flux in the volume element of the pond is also expressed by the following equation:

$$Q_{m,acc} = A_{pond} \Delta x \frac{\partial(\rho_{sw} S)}{\partial t} \quad (27)$$

So, the mass transfer process within the solar pond is governed by the following general differential equation:

$$\frac{\partial(\rho_{sw} S)}{\partial t} = D \frac{\partial^2(\rho_{sw} S)}{\partial^2 x} \quad (28)$$

All fluid properties vary as a function of both temperature and salinity and are evaluated using known formulae.

With the equation of state of the saline solution given as follows [31]:

$$\rho_{sw} = \rho_{ref}(1 - \alpha_{th}(T - T_{ref}) + \beta_m(S - S_{ref})) \quad (29)$$

$\alpha_{th}$  and  $\beta_m$  are thermal and salt expansion coefficients published in the literature. The subscripts 'ref' refers to the reference temperature of 25°C.

Finally, the process of mass and heat transfer in solar pond is described in the following system of equations:

$$\begin{cases} \frac{\partial(\rho_{sw} C p_{sw} T_{sw}(t, x))}{\partial t} = \lambda_{sw} \frac{\partial^2 T_{sw}(t, x)}{\partial^2 x} + 0,6 \mu_{ex} G_i e^{-\mu_{ex}(L-x)} \\ \frac{\partial(\rho_{sw} S)}{\partial t} = D \frac{\partial^2(\rho_{sw} S)}{\partial^2 x} \end{cases} \quad (30)$$

We developed a calculation program by using the Matlab software computation which solves the set of differential equations. We used the ode 45 function based on the explicit Runge-Kutta method. This function is generally used for the lower order systems. The resolution allows to determine the variations of the different temperatures and the daily distillate flow.

## Results and Discussion

### Solar radiation

The solar radiation model allows us to determine the instantaneous variation of different solar radiation for any day. Figure 3 represents the global solar radiation variation for the four typical days. Figure 3 shows that, for any day, the global solar flux follows the same shape. It increases from sunrise to reach a maximum at noon. It reaches a maximum of 980 W/m<sup>2</sup> at noon for the June 21, which is the highest while that of December is the lowest. Sunshine depends on the day and month, it is higher in summer.

After the theoretical modeling and simulation, experimental validation step is a milestone for the model performance evaluation and its subsequent exploitation. The Sunshine experimental values used for the model validation are taken using a station equipped with a sunshine Lambrecht installed in the region of Gabes (33.8933° of latitude and 10.1029° of longitude).

To validate the model results, a comparison between the simulated values and experimental data measured by our research team is made. Figure 4 shows a superposition of the two curves for the June 21. The present irregularity in the daily progress of the experimental curve is due to the cloudy crossing that could interrupt the running of experiments. The simulated values are a bit underestimated at the beginning and at the end of day.

The calculated average deviation between the two curves does not exceed 20%, while the average spread of solar flux is 38 W/m<sup>2</sup>. We can consider that the model correctly describes the evolution of the solar flux along the day. The results obtained in this section will be used for the simulations of the pond temperature variation.

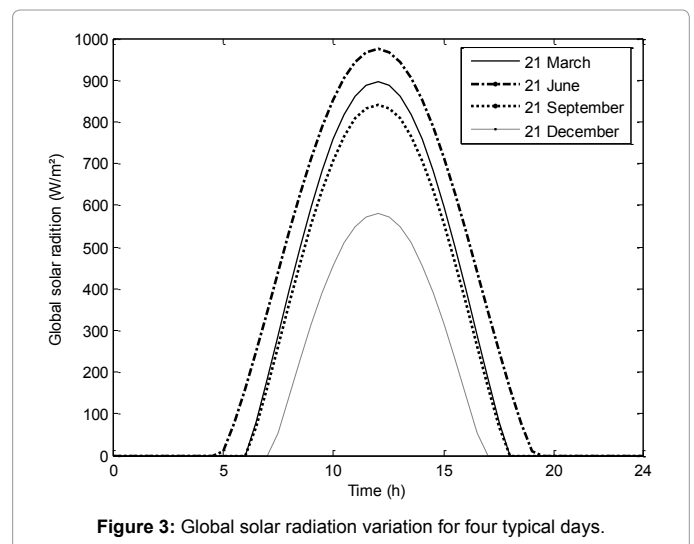
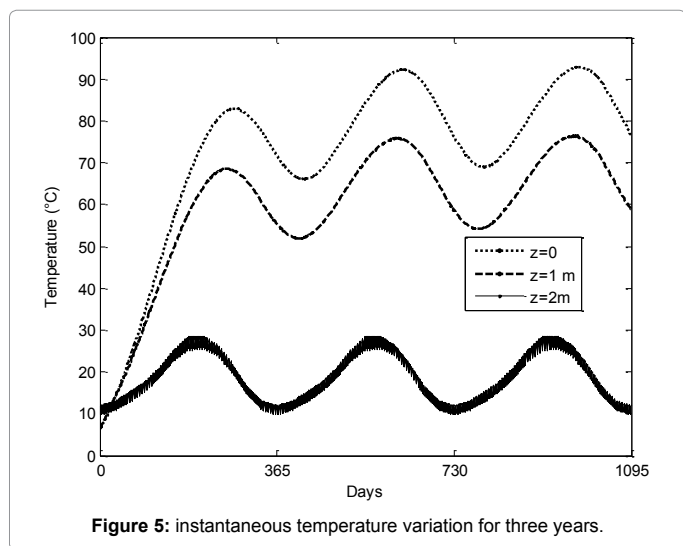
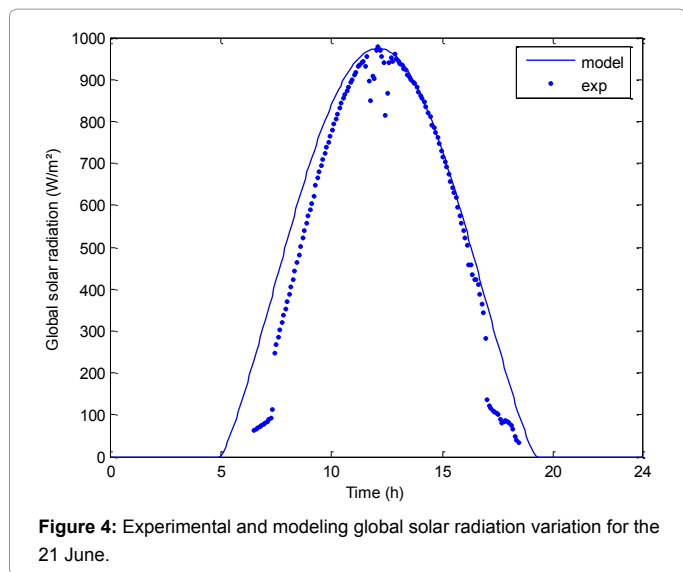


Figure 3: Global solar radiation variation for four typical days.



### Solar pond

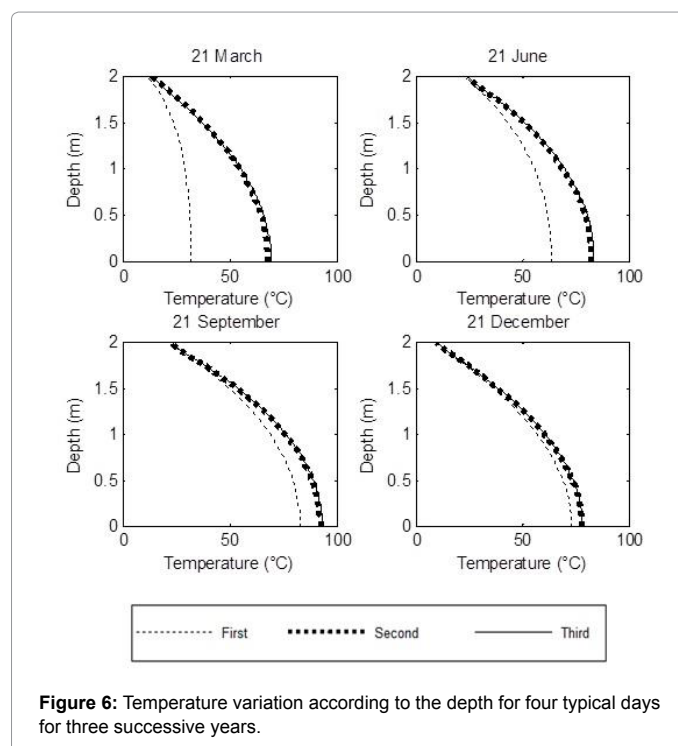
Solving the pond model equations allows determining the temperature instantaneous variation in the SGSP. The SGSP depth is of 2m. We propose to present the simulation results for three years of pond operation to interpret the pond behavior along time and study the stability and the effect of the energy accumulation. Figure 5 presents the instantaneous temperature variation for different depths in bottom of the pond ( $z=0\text{m}$ ), in the middle ( $z=1\text{m}$ ) and in the top ( $z=2\text{m}$ ). The SGSP operation started on 1<sup>st</sup>, January of the first year where the temperature in the SGSP was the ambient temperature. The temperature reaches its maximum during the summer when the solar radiation is maximal. The temperature at the end of the year is greater than that of the beginning, which is explained by the energy accumulation in the pond. Figure 5 shows that the upper zone temperature is near ambient temperature since the losses are higher in this zone. The temperature fluctuations at the interface that are due to variations in ambient temperature gradually disappeared, approaching the bottom of the pond. The highest temperature is the pond bottom; it is in the order of 95°C for the third year. For the same date, the temperature increases from one year to another due to the energy

stored in the pond. Consequently, the maximum temperature increases from 84°C for the first year to 92°C for the second year to 94°C for the third. So, this elevation decreases from one year to another until the temperature stabilizes at the end of the third year. Figure 6 presents the temperature according to the depth for four typical days for three successive years. It should be noted that these profiles were taken at a specific time, say at 12: 00h of each day.

Figure 6 shows that, when approaching the SGSP bottom, the temperature increases with the increase in salinity. Thus, the largest quantity of energy is absorbed by the concentrated salt solution at the bottom of the SGSP. Similarly, for the bottom, the temperature varies slowly so that the temperature becomes almost constant, thereby forming the LCZ zone. On the other hand, the temperature varies differently for four typical days, in which it varies slowly from one year to another in the cold months (September and December), while the variation is important for hot months (March and June). The solar heating effect within the pond is more important than for the cold season. Besides, for the cold season, in particular for the winter, heat losses towards the ambient temperature are more important due to cold air.

For the top portion (UCZ), the temperature is close to the ambient temperature. The cooling effect of water can be clearly observed in addition to the effect of the energy accumulated within the pond for March and June. This deviation disappeared for September and December, thus forming the UCZ zone.

For the intermediate portion (NCZ), the salinity increases with depth. This zone behaves as transparent heat insulation, and crossed by the solar radiation which is absorbed and trapped by the very salty water at the bottom. For this zone, the temperature profile remains essentially linear, then it slowly varies and the solar heating effect depends on the month. Despite the low ambient temperature and solar radiation for September, the temperature is higher than in June reaching 92°C. The solar heating effect due to the heat loss (low ambient temperature and



solar radiation) is about 5°C from September to December. Figure 6 shows that the temperature increase is important for March and June from the first to second year, whereas it does not exceed 5°C for December. Secondly, the temperature stabilizes in December of the third year.

Figure 7 displays salinity according to the depth for four typical days, showing the effects of temperature and heat diffusivity on the salinity variation. It is observed, at first, that the instantaneous salinity variation remains very low and seems almost imperceptible along the year. Thus, the profiles for the upper and central zone were nearly identical, except for the surface and the bottom zone where only a slight change can be noticed. So, the salinity varied slowly during the year reaching stability, thus the salinity profiles remained in the S form then it became linear.

### Module production

The fibres module characteristics were selected to support high temperatures at the membrane wall and have a good permeability. Table 1 shows the characteristics and operating conditions of hollow fibre module.

It is to be noted that the most important temperature is in LCZ part, exceeding 80°C which is the allowable temperature membrane. On the other hand, this zone is characterized by a high salinity, which presents a risk of clogging. For these two reasons, we came to the conclusion that the module feed or the module immersion in this zone is not recommended, hence we chose to couple the module with the middle part (NCZ). Therefore, two configurations were studied:

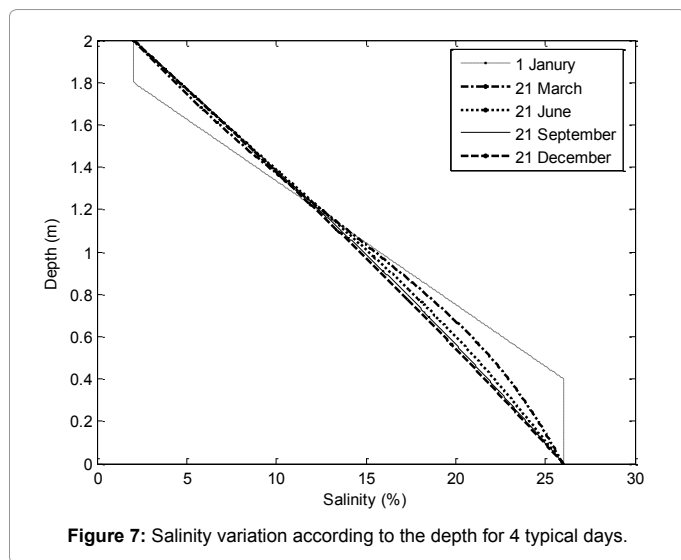


Figure 7: Salinity variation according to the depth for 4 typical days.

Nature	PVDF
Internal fibre diameter (mm)	2.6
Membrane thickness (mm)	0.4
Length (m)	1
Fibres number	18
Diameter module (cm)	2
Maximum temperature (°C)	80
Permeability (ms <sup>-1</sup> ) (T <sub>i</sub> in K)	$Km = 7.8 \cdot 10^{-6} \cdot T_i^{-0.5}$
Vacuum pressure (Pa)	4000
Water flow rate (m/s)	0.5

Table 1: Characteristics of hollow fibre module.

a hollow fiber module fed from the NCZ water and the hollow fiber module immersed in the NCZ zone.

Following the temperature, the permeate flow varied slightly along the day (Figure 8) such that it varies less than one kilogram along day. This permeate flow variation is related to the low variation of the temperature which does not exceed 1 to 2°C along the day. This low temperature variation is due to the energy accumulation in the pond which can be explained by the great inertia of the pond and the fact that the pond is stabilized after two operation years.

Table 2 shows that the highest daily production of the first year is that of June. However, the lowest production was that of March 21 because the temperature level was still low. Although the March solar radiation is higher than that of September and December, we can see that the production remains the lowest such that the March production for the third year is lower than that of December of the first year. On the other hand, the daily production of September is the greatest for the three year, reaching 346 kg per m<sup>2</sup> of membrane. This difference does not only depend on the temperature and the heat lost in the top of SGSP and the received solar flux, but also on the energy stored in the SGSP bottom. In fact, the March production was relative to previous months, which corresponds to low energy storage in winter months while the September production is relative to summer months. Consequently, the daily production increases from one year to another, especially for June and September, in which it multiplies of two times and half from the first year to the third.

To compare the two configurations of the fiber module, the daily production for the same operating conditions was calculated. Figure 9 reveals the daily production variation along three years. Module production began only at 80 days when the desired temperature level was reached. Indeed, the temperature did not exceed 30°C which is the evaporating temperature for 4000 Pa vacuum pressure. Figure 9 shows

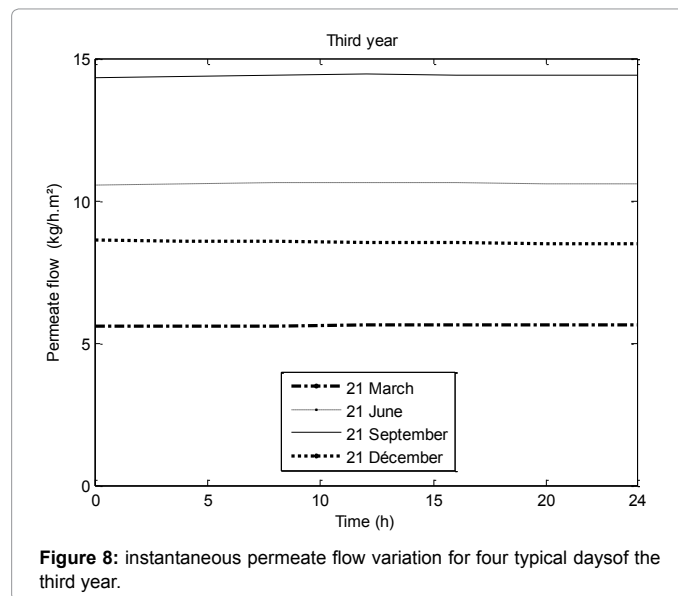


Figure 8: instantaneous permeate flow variation for four typical days of the third year.

Day	21-Mar	21-Jun	21-Sep	21-Dec
First year	3,5	100	242	163
Second year	125	243	339	202
Third year	135	255	346	205

Table 2: Daily separated module production for four typical days of three successive years (Kg/m<sup>2</sup>).

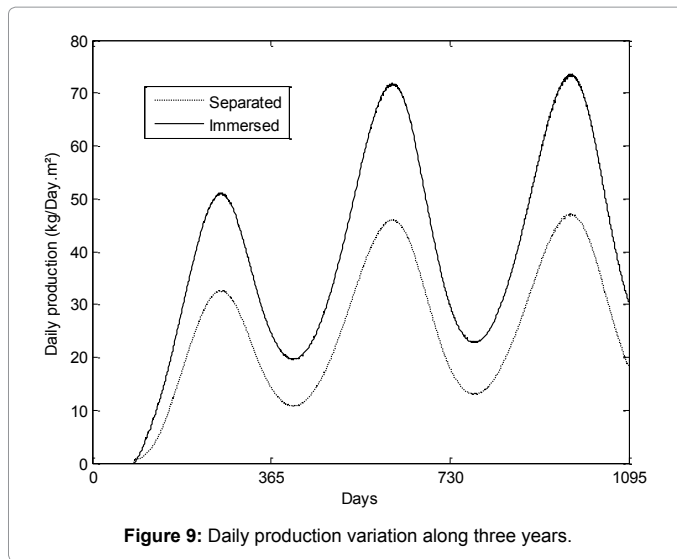


Figure 9: Daily production variation along three years.

that the daily production of the immersed module was greater than that of the separated module. The immersed module production presents more than one and a half times that of the separated module which exceeded the 75 kg/day per m<sup>2</sup> of membrane. This production presents an average productivity of 3.2 kg/h per m<sup>2</sup> of membrane which was close to that found by J.P. Mericq for a plan module immersed in SGSP (3.7 kg/h per m<sup>2</sup> of membrane) [21].

The third yearly immersed module production is 16.8 m<sup>3</sup> representing more than one and half times the separated module production. Thus, immersing the module in the solar pond improves the performance of the hollow fiber module.

## Conclusion

The present work theoretically investigates the possibility of coupling the DMV module with a SGSP. In order to study the contribution of solar energy effect and choose the most appropriate module configuration, a model describing the transfer in the module and the SGSP was developed. These models allow us to determine the instantaneous variation of hollow fiber module. The obtained results have confirmed that the daily production of the immersed module is higher than that of the separated module. It is to be noted that for this study, we have neglected the circulation conduit heat losses in the separated module, which is not the case for the immersed one, because the module immersion in the SGSP reduces the heat losses. Therefore, a more detailed study of the entire desalination system should be under taken in order to show the benefits of membrane module immersion in the SGSP. However, immersion is facing several technical limitations. Indeed, given that it must necessarily be put in contact with the module, it is necessary to use noble materials for the construction of the module. This problem does not arise in the case of the configuration where the membrane module is separated from the SGSP.

## References

- Khayet MM, Godino MP (2004) Heat and mass transfer in vacuum membrane distillation. *Int J Heat Mass Transfer* 47: 865-875.
- Cabassud CC, Lahoussine-Turcaud V (1998) A new process to remove halogenated VOCs for drinking water production: vacuum membrane distillation. *Desalination* 117.
- Darwish AN, Hilal N (2012) Membrane distillation. *Desalination* 287: 2-8.
- Jin Z, Yang DL, Jian XG (2008) Hydrophobic modification of poly (phthalazinone ether sulfone ketone) hollow fiber membrane for vacuum membrane distillation. *J Membrane Sci* 310: 20-27.
- Cabassud C, Wirth D (2002) Water desalination using membrane distillation: comparison between inside/out and outside/in permeation. *Desalination* 147: 139-145.
- Zuo G, Guan G, Wang R (2014) Numerical modeling and optimization of vacuum membrane distillation module for low-cost water production. *Desalination* 339: 1-9.
- Zrelli A, Chaouchi B, Gabsi S (2011) Simulation of vacuum membrane distillation coupled with solar energy: Optimization of the geometric configuration of a helically coiled fiber. *Desalin Water Treat* 36: 41-49.
- Mericq JP, Laborie S, Cabassud C (2010) Vacuum membrane distillation of seawater reverse osmosis brines. *Water Res* 44: 5260-5273.
- Abu-Zeid M, Zhang Y, Dong H, Hou L (2015) A comprehensive review of vacuum membrane distillation technique. *Desalination* 356: 1-14.
- Khayet M (2011) Membranes and theoretical modeling of membrane distillation: a review. *Advances Colloid Interface Sci* 164: 56-88.
- Sarbatly R, Chel-ken C (2013) Evaluation of geothermal energy in desalination by vacuum membrane distillation. *Appl Energy* 112: 737-746.
- Nakoa K, Kawtar R, Date A, Aliakbar A (2015) An experimental review on coupling of solar pond with membrane distillation. *Solar Energy* 119: 319-331.
- Susanto H (2011) Towards practical implementations of membrane distillation. *Chemical engineering and processing: Process intensification* 50: 139-150.
- Khayet M (2012) Solar desalination by membrane distillation: Dispersion in energy consumption analysis and water production costs (a review). *Desalination* 308: 89-101.
- Saffarini RB, Summer EK, Arafat HA, Lienhard VJH (2012) Economic evaluation of stand-alone solar powered membrane distillation systems. *Desalination* 299: 55-62.
- Banat F, Jwaied N, Rommel M, Wiegghaus M (2007) Performance evaluation of the "large SMADES" autonomous desalination solar-driven membrane distillation plant in Aqaba, Jordan. *Desalination* 217: 17-28.
- Shirazi MA, Kargari A (2015) Water Desalination: Solar-Assisted Membrane Distillation. *Encyclopedia of Energy Engineering and Technology* 2: 2095-2109.
- Wang X, Zhang L, Yang H, Chen H (2009) Feasibility research of potable water production via solar-heated hollow fiber membrane distillation system. *Desalination* 247: 403-411.
- Galvez JB, Garcia-Rodriguez L, Martin-Mateos I (2009) Seawater desalination by an innovative solar-powered membrane distillation system. *Desalination* 246: 567-576.
- Criscuoli A, Carnevale MC (2015) Desalination by vacuum membrane distillation: The role of cleaning on the permeate conductivity. *Desalination* 365: 213-219.
- Mericq JP, Laborie S, Cabassud C (2011) Evaluation of systems coupling vacuum membrane distillation and solar energy for sea water desalination. *Chemical Eng J* 166: 596-606.
- Abdallah SB, Frikha N, Gabsi S (2013) Simulation of solar vacuum membrane distillation unit. *Desalination* 324: 87-92.
- Zhang Y, Peng Y, Ji S, Chen P (2015) Review of thermal efficiency and heat recycling in membrane distillation processes. *Desalination* 367: 223-239.
- Abdallah SB, Frikha N, Gabsi S (2013) Study of the performances of different configurations of seawater desalination with a solar membrane distillation. *Desalination Water Treat* 52: 1-10.
- Lawson KW, Lloyd DR (1997) Membrane distillation. *J Membrane Sci* 124: 1-25.
- Sun L, Wang L, Wang Z, Wang S (2015) Characteristics analysis of cross flow vacuum membrane distillation process. *J Membrane Sci* 488: 30-39.
- Dao TD, Mericq JP, Laborie S, Cabassud C (2013) A new method for permeability measurement of hydrophobic membranes in Vacuum Membrane Distillation process. *Water Res* 47: 2096-2104.
- Climatic data handbook for Europe.

29. Mansour RB, Nguyen CT, Galanis N (2004) Numerical study of transient heat and mass transfer and stability in a salt-gradient solar pond. *Int J Ther Sci* 43: 779-790.
30. Alsaadi AS, Francis L, Amy GL, Ghaffour N (2014) Experimental and theoretical analyses of temperature polarization effect in vacuum membrane distillation. *J Membran Sci* 471: 138-148.
31. Mansour RB, Nguyen CT, Galanis N (2006) Transient heat and mass transfer and long-term stability of a salt-gradient solar pond. *Mechanics Res Commun* 33: 233-249.